

# Non-negative matrix factorization pansharpener: an application to mid-infrared astronomy

Olivier Berne, A. G. G. M. Tielens, Paolo Pilleri and Christine Joblin

**Abstract**—Mid-infrared astronomy (operating at wavelengths ranging from 2 to 25  $\mu\text{m}$ ) has progressed significantly in the last decades, thanks to the improvement of detector techniques and the growing diameter of telescopes. Space observatories benefit from the absence of atmospheric absorption, allowing to reach the very high sensitivities needed to perform 3D hyperspectral observations, but telescopes are limited in diameter ( $< 1$  meter) and therefore provide observations at low angular resolution (typically a few seconds of arc). On the other hand, ground-based facilities suffer from strong atmospheric absorption but use large telescopes (above 8m diameter) to perform sub-arcsecond angular resolution imaging through selected windows in the mid-infrared range. In this Paper, we present a method based on Lee and Seung's Non-negative Matrix Factorization (NMF) to merge data from space and ground based mid-infrared (mid-IR) telescopes in order to combine the best sensitivity, spectral coverage and angular resolution. We prove the efficiency of this technique when applied to real mid-IR astronomical data. We suggest that this method can be applied to any combination of low and high spatial resolution positive hyperspectral datasets, as long as the spectral variety of the data allows decomposition into components using NMF.

**Index Terms**—Astronomy, Telescopes, Spectroscopy, Signal processing, Hypercubes

## I. INTRODUCTION

In galaxies (including our own Galaxy, the Milky-Way), the ultraviolet (UV) and visible light (respectively wavelength ranges of 10-400 and 400-750 nm) emitted by stars is absorbed by dust particles having sizes ranging from a few nanometers to a few micrometers. The UV-visible energy they absorb is then re-emitted in the infrared (IR, 2-1000 $\mu\text{m}$  [1]). Therefore, in the recent years, astronomers have focused their efforts in studying the Milky-Way and external galaxies to the IR, where the emitted light contains information both on the amount of absorbed energy originating from stars and on the composition of interstellar dust. Unfortunately, most of the IR light coming from space is absorbed by the atmosphere. This has motivated a number of IR space missions that provide the sensitivity required to perform hyperspectral observations. However, due to technical and cost constraints, space mission can only launch small diameter telescopes, which limits the spatial resolution

Olivier Berné and A. G. G. M. Tielens are with the Leiden Observatory, P.O. Box 9513 NL-2300 RA Leiden, The Netherlands

Paolo Pilleri and Christine Joblin are with the Université de Toulouse ; UPS ; CESR ; 9 ave colonel Roche, F-31028 Toulouse cedex 9, France, CNRS; UMR 5187; 31028 Toulouse, France

This work is based on observations made with the Spitzer Space Telescope, which is operated by the Jet Propulsion Laboratory, California Institute of Technology under NASA contract 1407.

This work has been submitted to the IEEE for possible publication. Copyright may be transferred without notice, after which this version may no longer be accessible.

of the obtained data. Conversely, the ground-based telescopes working in the IR usually have large apertures providing subarcsecond angular resolution, but low sensitivities, that only permit imaging through a few broad band filters. In the field of remote sensing, a set of methods referred to as *pansharpener* [2] have been developed in order to perform data fusion/improvement by combining hyperspectral datasets at different spatial resolutions. In this paper, we present such a method, developed to combine ground and space data, to benefit from the advantages of the two techniques. This method is based on the decomposition into *components* of hyperspectral data obtained by space telescopes, using Non-Negative Matrix Factorization (NMF), followed by non-negative least square fitting of ground-based data using these *components* (Sect.II). We apply this to real data obtained in the mid-IR range (5-15  $\mu\text{m}$ ) in order to prove the efficiency of the proposed method (Sect.III).

## II. FORMALISM

### A. Decomposition into components with NMF

We define the hyperspectral observations of a region of the sky as a 3 dimensional  $m_s \times n_s \times l_s$  matrix  $C_s(x, y, \lambda)$  where  $(x, y)$  define the spatial coordinates and  $\lambda$  the spectral index. We assume that all the points in  $C_s(x, y, \lambda)$  are positive. We call *spectrum* each vector  $x_s(p_x, p_y, \lambda)$  recorded at a position  $(p_x, p_y)$  over the  $l_s$  wavelength points. We define a new positive 2D matrix of observations  $X_s$ , the rows of which contain the  $m_s \times n_s = k_s$ ,  $x_s$  spectra of  $C_s$ . We now assume that each *spectrum*  $x_s$  is the result of a linear combination of a limited number  $r_s$ , with  $r_s \ll k_s$ , of unknown *source spectra* written  $s_s(\lambda)$  so that:

$$x_s(p_x, p_y, \lambda) = \sum_{i=1 \dots r_s} a^i(p_x, p_y) s_s^i(\lambda), \quad (1)$$

where the  $a^i(p_x, p_y)$  coefficients are unknown. This can be re-written under the following matrix product:

$$X_s = A_s \times S_s, \quad (2)$$

where  $A_s$  is the  $k_s \times r_s$  matrix of unknown coefficients of the linear combinations and  $S_s$  is an  $r_s \times l_s$  matrix, the rows of which are the *source spectra*. This is a typical blind source separation (BSS) problem [3], and can be solved using multiple methods (e.g. [4], [5], [6]). Here, we concentrate on Non-Negative matrix factorization [4] that is applicable because  $A$  and  $S$  are positive. The objective is to find estimations of  $A_s$  and  $S_s$ , respectively  $W_s$  and  $H_s$  so that

$$X_s \approx W_s \times H_s. \quad (3)$$

This is done by adapting the non-negative matrices  $W_s$  and  $H_s$  so as to minimise the squared Euclidian distance  $\|X_s - W_s H_s\|^2$  or the divergence  $D(X_s|W_s H_s)$ , respectively defined as

$$\|X_s - W_s H_s\|^2 = \sum_{ij} (X_s^{ij} - (W_s H_s)^{ij})^2, \quad (4)$$

and

$$D(X_s|W_s H_s) = \sum_{ij} (X_s^{ij} \log \frac{X_s^{ij}}{(W_s H_s)^{ij}} - X_s^{ij} + (W_s H_s)^{ij}), \quad (5)$$

$$-X_s^{ij} + (W_s H_s)^{ij}), \quad (6)$$

where the exponents  $i$  and  $j$  respectively refer to the row and column indexes of the matrices. The algorithm used to achieve the minimisation of the Euclidian distance is based on the iterative update rule

$$\begin{aligned} H_s &\leftarrow H_s \frac{({}^T W_s X_s)}{({}^T W_s W_s H_s)}, \\ W_s &\leftarrow W_s \frac{(X_s {}^T H_s)}{(W_s H_s {}^T H_s)} \end{aligned} \quad (7)$$

and for divergence

$$\begin{aligned} H_s &\leftarrow H_s \frac{\sum_i W_s^i X_s^i / (W_s H_s)^i}{\sum_j W_s^j}, \\ W_s &\leftarrow W_s \frac{\sum_i H_s^i X_s^i / (W_s H_s)^i}{\sum_j H_s^j}. \end{aligned} \quad (8)$$

Euclidian distance and divergence are non increasing under their respective update rules, so that starting from random  $W_s$  and  $H_s$  matrices, the algorithm will converge towards a minimum for these criteria. This provides the matrix  $H_s$  containing the  $r_s$  estimated *source spectra*.

### B. Panshaping

Once this step has been achieved, one can observe the same region, with a much higher spatial resolution, but much fewer points in wavelength. This is typically what is done in the mid-IR from ground-based telescopes. This will provide a new hyperspectral cube  $C_g(x, y, \lambda)$  with  $k_g = m_g \times n_g \gg m_s \times n_s$  spatial positions and  $l_g \ll l_s$  spectral points. As in Sect. II-A, we define an observation matrix  $X_g$  that contains the *spectra* of  $C_g$ . Again we assume that each spectrum in  $X_g$  can be approximated using a linear combination of  $r_g$  *source spectra*  $s_g$  with  $l_g$  points. In matrix form, this read:

$$X_g \approx W_g \times H_g, \quad (9)$$

where  $X_g$  is the matrix of spectra observed from the ground,  $H_g$  is the matrix of *source spectra*, and  $W_g$  a matrix of unknown coefficients. In fact, the *source spectra* over  $l_s$  spectral points have already been estimated above using NMF and are given by  $H_s$ . Because the same region is being observed, the *source spectra* in  $H_g$  are expected to be the same as those in  $H_s$  but recorder over  $l_g$  spectral positions. Therefore, we construct  $H_g$  by taking the points in  $H_s$  corresponding to the  $l_g$  spectral positions. Now that  $X_g$  and  $H_g$  are known, Eq. 9 no

longer defines a BSS problem and  $W_g$  can easily be adjusted by least square methods [7]. At the end of this process we therefore have in  $W_g$  the  $k_g$  coefficients by which the  $H_g$  matrix has to be multiplied to recover the observed spectrum. Instead, one can build a new *panshaped* matrix  $X_p$  defined by:

$$X_p = W_g \times H_s. \quad (10)$$

This matrix contains the spectra for  $k_g$  spatial positions and  $l_s$  wavelength points. Finally, the *spectra* in the  $X_p$  matrix can be reassigned their respective positions in an  $m_g \times n_g \times l_s$  hyperspectral cube  $C_p(x, y, \lambda)$ . The  $C_p$  cube has therefore the high number of spatial points of  $C_g$  and high number of points in wavelength of  $C_s$ .

## III. APPLICATION TO REAL DATA

In order to test the above method we have applied it to real astronomical data of the NGC 7023 nebula. The observed set that will serve as reference (Fig. 1.d) is a spectral cube  $C_{ref}$  obtained by the Spitzer space Telescope [8] recorded over  $36 \times 28$  spatial positions and 180 points in wavelength in the mid-IR (5-14  $\mu\text{m}$ ). We simulate a low spatial resolution cube by degrading the spatial resolution of  $C_{ref}$  by a factor of 4. This provides  $C_s$  that has  $9 \times 7$  spatial points but still 180 points in wavelength (Fig. 1.a).  $C_g$  is constructed by keeping only 10 points in wavelengths of  $C_{ref}$ , corresponding to windows that can be observed from the ground, but with the full spatial resolution.  $C_g$  has  $36 \times 28$  spatial points but only 10 spectral positions (Fig. 1.b). The first step consists in applying NMF to  $C_s$  as described in Sect. II-A. In order to do this, the number of rows  $r_s$  of  $H_s$  has to be set. To do this we apply NMF for successive values of  $r_s$  and keep the smallest value that provides:

$$\sum_{i,j} (X_s - W_s \times H_s)^2 \sim \sum_{i,j} N_s^2 \quad (11)$$

where  $N_s$  represents additive contribution of noise to signal in  $C_s$ . We find that  $r_s = 3$  satisfies the above statement, and the 3 obtained spectra of  $H_s$  are presented in Fig. 1.a. In the present application, each of the obtained *source spectra* can be attributed to the emission of different chemical species: neutral and ionized polycyclic aromatic hydrocarbon molecules (resp. PAH<sup>0</sup> and PAH<sup>+</sup>) and very small carbonaceous grains (VSG). This attribution has been discussed in [9] and [10] and is beyond the scope of the present paper. However, we will keep these acronyms in the following for practical reasons. Using the obtained  $H_s$  matrix, we construct the  $H_g$  matrix following the strategy explained in Sect. II-B. Using the Non Negative Least Square (NNLS) algorithm [7], we identify the values of the coefficients in  $W_g$ . Finally, using equation 10 we build  $X_p$  from  $W_g$  and  $H_s$ . We then reshape  $X_p$  in order to recover a spectral cube  $C_p$  with  $36 \times 28$  spatial positions and 180 points (Fig. 1. c).

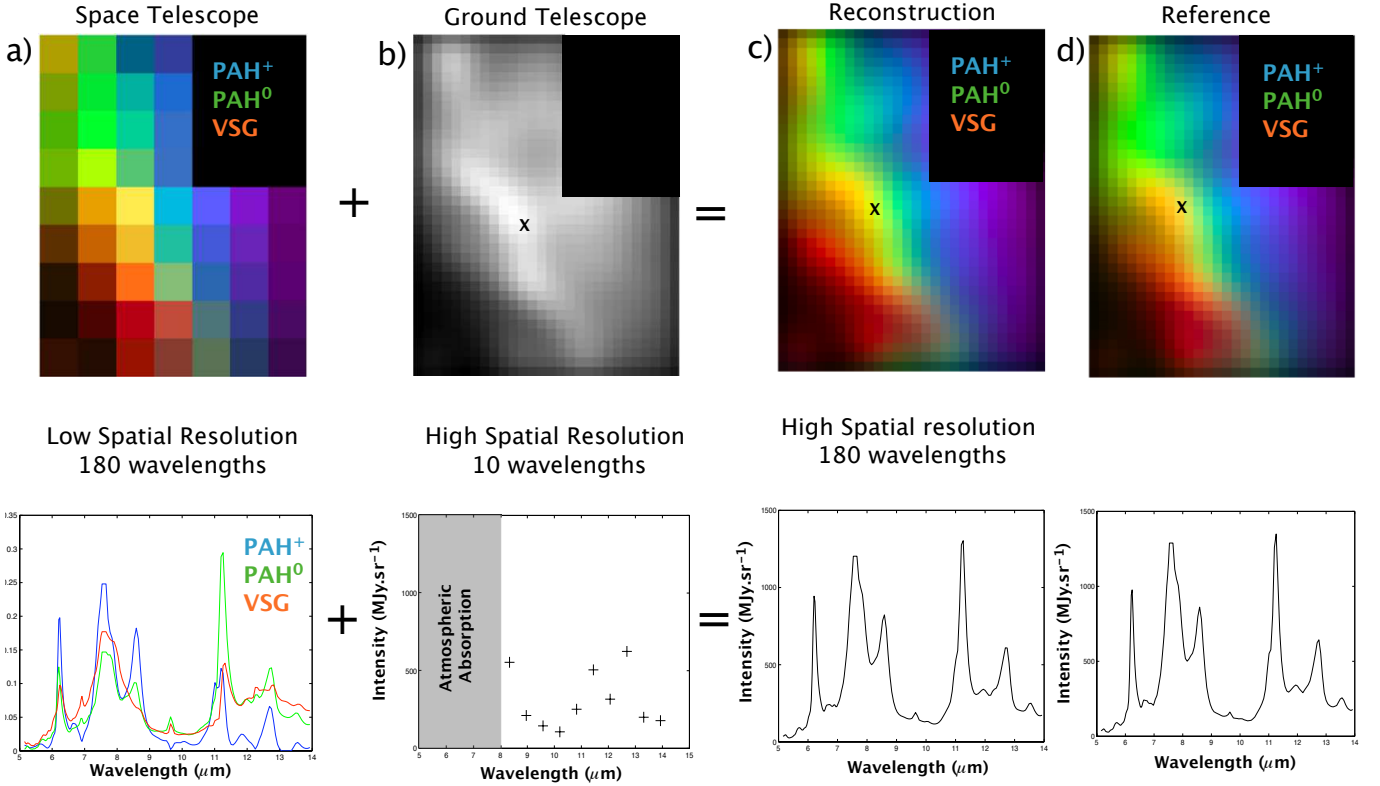


Fig. 1. Illustration of the steps achieved to perform pansharping on mid-IR data of the NGC 7023 nebula: **a)** Application of non-negative matrix factorization to the low spatial resolution  $C_s$  cube. The *source spectra* in  $H_s$ : PAH<sup>0</sup>, PAH<sup>+</sup> and VSG are shown in the lower panel. The colors in the upper image show the respective contribution, given by  $W_s$ , of these three *source spectra* in the  $C_s$  cube at each spatial position. Colors combine as standard RGB i.e. green+red=yellow etc. **b)** Upper: image at high spatial resolution taken at a given wavelength position from the  $C_g$  cube. Lower panel shows the spectra at position indicated by a cross in the image. **c)** High spatial/septal resolution  $C_p$  cube obtained using NMF pansharping. The contribution of each *source spectrum* from  $H_s$  at each spatial position is given with RGB colors as for the  $C_s$  cube. Lower panel shows the reconstructed full mid-IR spectrum at the position indicated on the image by a cross. **d)** Reference cube  $C_{ref}$ . The colors show the contribution of each *source spectra* from  $H_s$  to the mid-IR spectrum at each spatial position, obtained by NNLS. Lower panel shows the reference *spectrum* at the position indicated by a cross in the image. In all panels, the black mask in the upper right-hand corner of the images is used to mask the contribution from a bright star.

### A. Efficiency of the method

The efficiency of the proposed method can be estimated by comparing  $C_p$  and  $C_{ref}$ . Visually, the reconstruction seems very efficient (See Fig. 1 c)) and d)) for the spatial distribution of the *source spectra*. Fig. 2 shows an overlay of the original observed spectrum at the position marked with a cross in Fig. 1 and the reconstructed spectrum. The match is excellent. Quantitatively, we can estimate the reconstruction efficiency of our method,  $Q$ , defined by:

$$Q = \sqrt{\frac{[\sum_{x_i, y_j} \int (C_p - C_{ref})^2 d\lambda]}{[\sum_{x_i, y_j} \int C_{ref}^2 d\lambda]}}, \quad (12)$$

which compares the norm of the residuals cube  $C_p - C_{ref}$  and the norm in the reference cube  $C_{ref}$ . We find that  $Q \sim 0.09$  meaning that the average reconstruction precision is 9% which is similar to the intrinsic uncertainty present in the  $C_{ref}$

data. The full application presented above was implemented under Matlab. Given that this method only involves multiplicative calculation, the whole process NMF+Pansharping runs in less than a minute on a laptop computer. We however note that this method will only perform for datasets which show significant spectral variations, i.e. providing a variety of observed mixtures that is sufficient to achieve NMF. Furthermore, the number of spectral points obtained in the high spatial resolution dataset must be sufficient (typically about 10) to allow a unique solution to NNLS fitting.

### B. Astrophysical implications

We have proven the efficiency of the proposed method to obtain "pansharped" cubes with full spatial and spectral samplings, combining data from space and ground-based observatories. This has several advantages for astronomical observations:

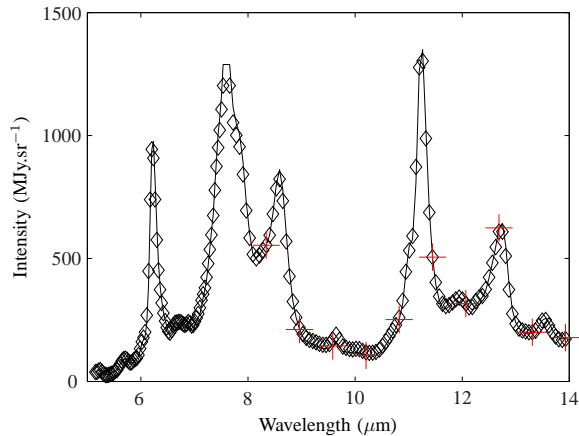


Fig. 2. A 10 points spectrum taken from  $C_g$  at the position marked with a cross in Fig. 1 (red crosses). The continuous line shows the spectrum taken from  $C_p$  at the same position, reconstructed by fitting the ten points with a linear combination of *source spectra*. In diamonds is the reference spectrum taken in  $C_{ref}$  at the same position.

- Astronomical spectra are always positive so this method can easily be applied.

- The method is shown to increase the spatial resolution of mid-IR hyperspectral observations obtained by space telescopes (here by a factor 4).

- The method can provide the full mid-IR spectrum, including in the spectral region that not accessible from the ground.

- The proposed technique can yield spatially resolved mid-IR hyperspectral observations of astronomical objects for which it would be impossible by classical techniques.

- The procedure involves only multiplicative computations, so is easy to implement and fast.

The next step consists in obtaining real mid-IR high angular resolution data from a ground-based telescope, for astronomical objects previously observed with the Spitzer Space Telescope. We have obtained 10 hours of telescope time on the largest single aperture telescope in the world, the Grantecan (GTC) telescope, in order to do this. We will then be able to combine Spitzer and GTC observations using non-negative matrix pansharping. This will provide the highest angular resolution (0.2 arcseconds) mid-IR spectral cube ever obtained for an astronomical object.

#### IV. CONCLUSION

We have proposed an NMF-based pansharping method that allows to benefit from the high spatial resolution of mid-IR instruments in ground-based observatories and sensitivity and spectral coverage of space telescopes. The only working hypothesis is that the data is positive, which in the case of remote sensing is usually the case. We have successfully applied this technique to real astronomical observations. Promising applications could be performed in the context of future ground- and space-based mid-IR missions. In particular, the NASA James Webb Space Telescope (JWST hereafter) and SPICA (JAXA) space missions will provide mid-IR spectral cubes at angular resolutions of 0.2 arcseconds. Meanwhile, the future

ground-based, 42 meters, European Large Telescope (ELT hereafter) will observe at milliarcsecond angular resolutions. The combination of JWST/SPICA data with ELT data using NMF pansharping will provide data at the scale size of, for example, the habitable zone of planet forming disks around young stellar objects. Finally, we emphasize the fact that NMF pansharping can well be apply to any combination of low and high spatial resolution hyperspectral datasets for which an NMF decomposition into parts is found.

#### ACKNOWLEDGMENT

The authors would like to thank the French PCMI program for financial support.

#### REFERENCES

- [1] B. T. Draine, "Interstellar Dust Grains," *Annual Reviews of Astronomy and Astrophysics*, vol. 41, pp. 241–289, 2003.
- [2] L. Alparone, L. Wald, J. Chanussot, C. Thomas, P. Gamba, and L. M. Bruce, "Comparison of pansharping algorithms: Outcome of the 2006 GRS-S data-fusion contest," *IEEE TRANSACTIONS ON GEOSCIENCE AND REMOTE SENSING*, vol. 45, no. 10, pp. 3012–3021, OCT 2007.
- [3] J. Cardoso, "Blind signal separation: Statistical principles," *PROCEEDINGS OF THE IEEE*, vol. 86, no. 10, pp. 2009–2025, OCT 1998.
- [4] D. D. Lee and H. S. Seung, "Algorithms for non-negative matrix factorization," in *NIPS*, MIT press, Ed., vol. 13, 2001, p. 556.
- [5] A. Hyvarinen, "A Fast Robust Fixed Point Algorithm for Independant Component Analysis," *IEEE Transactions on Neural Networks*, vol. 10, pp. 626–934, 1999.
- [6] R. Gribonval, "A survey of sparse component ananlysis for blind source separation : principles, perspectives and new challanges." in *Proceedings of ESANN 06*, 2006, pp. 323–330.
- [7] C. L. Lawson and R. J. Hanson, *Solving least squares problems*. Prentice-Hall Series in Automatic Computation, Englewood Cliffs: Prentice-Hall, 1974, 1974.
- [8] Werner, M. J. et al., "The Spitzer Space Telescope Mission," *Astrophysical Journal Supplement Series*, vol. 154, pp. 1–9, Sep. 2004.
- [9] M. Rapacioli, C. Joblin, and P. Boissel, "Spectroscopy of polycyclic aromatic hydrocarbons and very small grains in photodissociation regions," *Astronomy & Astrophysics*, vol. 429, pp. 193–204, Jan. 2005.
- [10] O. Berné, C. Joblin, Y. Deville, J. D. Smith, M. Rapacioli, J. P. Bernard, J. Thomas, W. Reach, and A. Abergel, "Analysis of the emission of very small dust particles from Spitzer spectro-imagery data using blind signal separation methods," *Astronomy & Astrophysics*, vol. 469, pp. 575–586, Jul. 2007.